JASR 6759
TYPED/ 10/4/04
ARTICLE IN PRESS
No. of pages: 6
DTD 4.3.1 / SPS-N

Available online at www.sciencedirect.com
SCIENCE DIRECT®

Advances in Space Research xxx (2004) xxx–xxx

ADVANCES IN SPACE RESEARCH
(a COSPAR publication)

www.elsevier.com/locate/asr

NLC detection and particle size determination: first results from SCIAMACHY on ENVISAT

C. von Savigny [a,*], A. Kokhanovsky [a,b], H. Bovensmann [a], K.-U. Eichmann [a], J. Kaiser [a,c], S. Noël [a], A.V. Rozanov [a], J. Skupin [a], J.P. Burrows [a]

[a] Institute of Environmental Physics/Remote Sensing (iup/ife), University of Bremen, Otto-Hahn-Allee 1, 28334 Bremen, Germany
[b] Institute of Physics, 70 Skarina Avenue, Minsk 220072, Belarus
[c] Remote Sensing Laboratories, University of Zurich, Winterthurerstr. 190, 8006 Zurich, Switzerland

Received 1 December 2002; received in revised form 1 May 2003; accepted 23 May 2003

Abstract

Measurements of limb scattered radiance spectra performed with the SCanning Imaging Absorption SpectroMeter for Atmospheric CHartographY (SCIAMACHY) aboard ENVISAT are used to detect noctilucent clouds (NLCs) in the northern hemisphere during summer 2002. The NLCs are easily identified by enhanced limb radiances around 80 km tangent height. Using limb radiances in the UV-B/C spectral range, where multiple scattering is negligible, the spectral signature of the NLC backscatter can be determined directly. Mie-calculations are used to estimate particle sizes of these clouds from SCIAMACHY measurements. In particular, we use the information contained in the spectral exponent of the NLC limb backscatter signal. The derived particle radii assuming a log-normal NLC particle size distribution are 40–50 nm and they are in excellent agreement with previous particle size estimates.

Keywords: Noctilucent clouds; Limb scattered radiance spectra; Particle sizes; SCIAMACHY; ENVISAT

1. Introduction

The summer mesosphere still receives a significant amount of scientific interest, particularly related to noctilucent clouds. NLCs occur near 82 km altitude during about a 12 week period centered 2 weeks after summer solstice in the summer hemisphere, poleward of about 55° (Thomas and Oliviero, 1989), where temperatures frequently drop below 150 K. The particles predominantly consist of water ice (Hervig et al., 2001) with radii ranging from about 10 nm to about 80 nm (e.g., Witt et al., 1976; Rusch et al., 1991; Gumbel et al., 1999; von Cossart et al., 1999). Larger radii (up to 350 nm) have also been reported (Thomas, 1991). The study of NLCs with UV/vis optical methods has a history of several decades. NLCs were detected with limb viewing satellite spectrometers (OGO 4 (Donahue et al., 1972), UVS on SME (Thomas and Oliviero, 1989), OSIRIS on Odin (e.g., Petelina et al., 2001)) and imagers (WINDII on UARS (e.g., Evans et al., 1995)), rocket-borne photometers and polarimeters (e.g., Witt et al., 1960; Gumbel et al., 2001) and ground-based LIDARs (e.g., von Cossart et al., 1999; Alpers et al., 2000). The estimation of NLC particle sizes is possible from measurements of color ratios of the NLC backscatter signal (e.g., Rusch et al., 1991; von Cossart et al., 1999), the NLC extinction spectrum in solar occultation (Debrestian et al., 1997) and from measurements of the NLC scattering phase function with photometers on spinning rockets (Witt et al., 1976; Gumbel et al., 2001). Gumbel and Witt (2001) showed in a case study that the particle size estimation by color ratios and measurement of the phase function yield consistent results. Recently, the determination of both radius and width of an assumed log-normal particle size distribution became possible with multi-wavelength LIDAR measurements. In this

* Corresponding author. Tel.: +49-421-218-4582; fax: +49-421-218-4555.
E-mail address: csavigny@iup.physik.uni-bremen.de (C. von Savigny).

0273-1177/$30 © 2004 COSPAR. Published by Elsevier Ltd. All rights reserved.
doi:10.1016/j.asr.2003.05.050

context, von Cossart et al. (1999) studied 11 NLC events over Andoya (Norway) with a 3-wavelength LIDAR system. They assumed that the NLC particles are water ice spheres, having a log-normal particle size distribution (PSD)

$$f(r) = \frac{N}{\sqrt{2\pi} r \ln\sigma} e^{-\frac{\ln^2(r/r_0)}{2\ln^2\sigma}} \quad (1)$$

where N is the number density of NLC particles and r is the radius of a particle. Using Mie-theory, von Cossart et al. (1999) found values of $r_0 = 51 \pm 21$ nm and $\alpha = 1.42 \pm 0.22$ for the 11 events. They also estimated the particle number density and obtained a value of $N = 82 \pm 52$ cm^{-3} based on their assumptions. To what extent the non-sphericity of the NLC particles (Baumgarten et al., 2002) and their refractive index influence the retrieval results remains unclear.

Each NLC observation method has its advantages and disadvantages: LIDARs and rocket photometers generally have a much higher vertical resolution (usually better than about 200 m) than limb viewing satellite-based instruments (typically 1–3 km). Rocket-borne instruments provide measurements at a single point in space and time only, whereas LIDAR measurements can in principle provide an extended temporal record of NLC presence, altitude, and particle size estimate for a given location. The advantage of satellite observations is their ability to provide a global picture of NLC occurrence and particle size estimates. The exact altitude of NLCs cannot be determined with limb scattered sunlight observations, only an upper limit can be established. Moreover, observations with sun-synchronous satellites cannot provide information on the local solar time dependence of atmospheric phenomena, since air volumes at a certain latitude are always sampled at the same local solar time.

The purpose of this paper is to present preliminary results of NLC observations and particle size estimates from SCIAMACHY limb measurements and to show that SCIAMACHY with its global coverage and its wide spectral range has the capability to significantly improve our understanding of the summer mesosphere.

2. Brief instrumental description

SCIAMACHY is one of 10 scientific instruments on board the European Space Agency's ENVISAT satellite. ENVISAT was launched on March 1st 2002 from Kurou (French Guyana) into a sun-synchronous polar orbit with an inclination of 97.8° and a descending node at 10:30 local solar time. SCIAMACHY is the first instrument capable of performing spectroscopic observations of the Earth's atmosphere in three observation modes: nadir viewing mode, limb viewing mode, as well as the solar and lunar occultation modes. For this study only SCIAMACHY limb observations were employed. SCIAMACHY has eight channels each of which contains a grating. The spectral range between about 220 and 2380 nm is covered with a spectral resolution of about 0.2 nm in the UV-B/C spectral range relevant to this study. In the limb observation mode the Earth's limb is stepped through for a tangent height range between −3 and 100 km in steps of about 3.3 km. After each tangent height step an azimuthal scan is performed covering a distance of about 960 km at the tangent point. The entire atmosphere from the troposphere up to the mesopause is observed all the time. Thus, no dedicated summer mesosphere campaign is necessary for the observation of NLCs. SCIAMACHY's instantaneous field of view spans 2.6 km vertically and 110 km horizontally at the tangent point. Further information on the instrument, measurement modes and mission goals was given by Bovensmann et al. (1999).

3. Methodology

For the NLC studies presented here SCIAMACHY limb radiance observations in the UV spectral range (channel 1, covering the range from about 220–310 nm) were employed. The use of UV wavelengths is advantageous compared to visible wavelengths, and this is why the UV spectral range has been intensively used for NLC studies (e.g., Witt et al., 1976; Gumbel and Witt, 2001; Gumbel et al., 2001). Due to the strong absorption within the Hartley and Huggins bands of ozone the detected limb scattered photons have almost exclusively experienced only one scattering event (e.g., Kaiser and Burrows, 2002). The single scattering approximation (Kokhanovsky, 2001) is therefore sufficient to interpret the measurements. This also implies that the ground albedo has no impact on the observed radiances. Therefore, the spectral signature of the NLC backscatter can be determined with high accuracy.

Fig. 1 shows examples of SCIAMACHY limb radiance profiles at several UV wavelengths with NLCs within the field of view (FOV) (panel a), and without NLCs in the FOV (panel b). In the absence of NLCs the limb radiance increases with decreasing tangent height as long as one is within the optically thin regime, i.e., the line of sight (LOS) optical depth τ is small. The observed limb radiance consists of different contributions in the presence of NLCs: (a) the molecular Rayleigh background; (b) backscatter signal from the NLC. The limb radiance profiles in Fig. 1b exhibit a maximum (the so-called "knee") between about 50 and 70 km depending on the wavelength. This is indicative of a LOS optical depth exceeding a certain threshold ($\tau \gg 1$). The atmosphere becomes optically thick, i.e., the transmission from the tangent point to the observer is close to zero. The knee altitude is only weakly dependent on geo-lo-

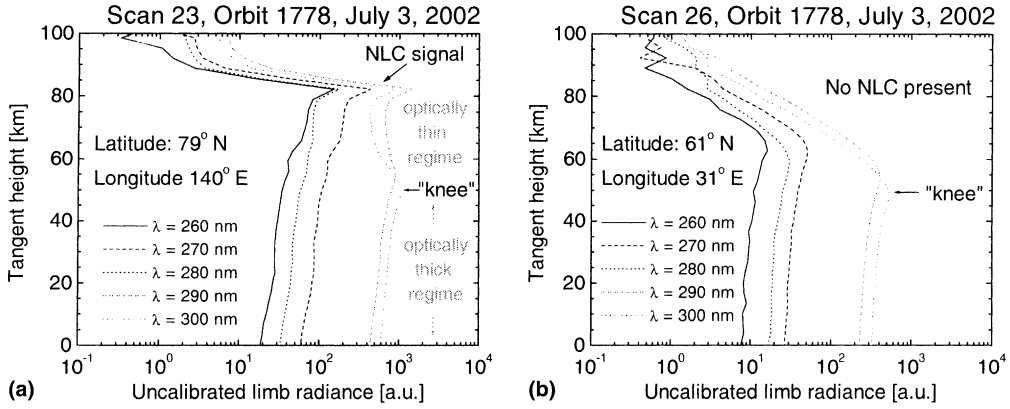

Fig. 1. Examples of UV limb radiance profiles observed with SCIAMACHY: (a) with NLCs; (b) without NLCs in the field of view.

cation and geophysical parameters and has therefore also been employed for attitude determination of limb sensors (e.g., Sioris et al., 2001).

For this study Level 0 data were used that have been corrected for dark current and responsivity. The instrument's polarization sensitivity is not taken into account, but this has a negligible effect on the limb radiance profiles, since the degree of linear polarization is almost independent of tangent height, as confirmed with the spherical vector radiative transfer model of McLinden et al. (2002).

Fig. 2 shows a polar plot, of all NLCs detected with SCIAMACHY on August 11, 2002. Note that the data of only 10 of the 14 orbits performed on this particular day were available and are shown in Fig. 2. The rectangles correspond to the area covered by the tangent point ground track for each limb scan. The presence of NLCs is indicated by solid black rectangles, hatched rectangles are NLC free. Obviously, NLCs only cover the highest latitudes on August 11, typical for the retraction of NLCs to higher latitudes at the end of the NLC season.

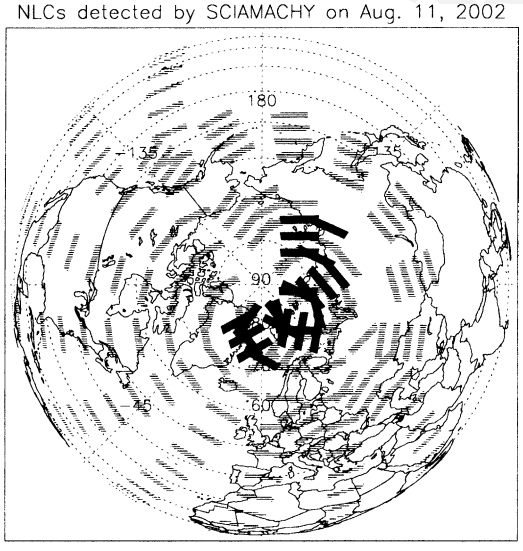

Fig. 2. NLCs detected by SCIAMACHY on August 11, 2002 are depicted by solid black rectangles. Hatched rectangles correspond to SCIAMACHY limb scans where no NLC was detected.

The NLCs are optically thin with visible slant peak optical depths of typically less than 5×10^{-3} (Debrestian et al., 1997). The total UV–Vis LOS optical depth from the tangent point at a tangent height of 82 km (the typical altitude of NLCs) to an observer in space is smaller than 5×10^{-2}. This is valid even in the center of the O_3 Hartley bands near 250 nm. In the single scattering approximation the contribution of the observed limb radiance $I_{\mathrm{NLC}}(\lambda, \Theta)$ originating from scattering by the NLC can be calculated in the following way (Kokhanovsky, 2001)

$$I_{\mathrm{NLC}}(\lambda, \Theta) = A \times q(\lambda, \Theta) \times S(\lambda), \quad (2)$$

where $q(\lambda, \Theta)$ is the NLC differential scattering coefficient, Θ denotes the scattering angle, $S(\lambda)$ is the solar spectrum, and A corresponds to a spectrally neutral proportionality constant. Employing longer, i.e., visible wavelengths is in principle desirable, since then both parameters of an assumed log-normal particle size distribution (see Eq. (1)) can in principle be determined (Alpers et al., 2000; von Cossart et al., 1999). Yet, the multiple scattering source function has to be taken into account and this will generally not be known with sufficient accuracy, since surface albedo and cloud cover would have to be known and modeled exactly.

The NLC sun-normalized limb scatter spectrum $i(\lambda, \Theta) = \frac{I_{\mathrm{NLC}}(\lambda, \Theta)}{S(\lambda)}$, which is proportional to $q(\lambda, \Theta)$. was derived (see Eq. (2)) at wavelengths in the UV-B and UV-C (265–300 nm). 265 nm was chosen as the lower boundary to avoid contamination by the stronger NO γ-bands at shorter wavelengths. The Rayleigh background was determined from model calculations with the radiative transfer model SCIARAYS (Kaiser, 2001). The simulated limb radiance profiles were scaled to match the observed limb radiance profiles at the "knee". The

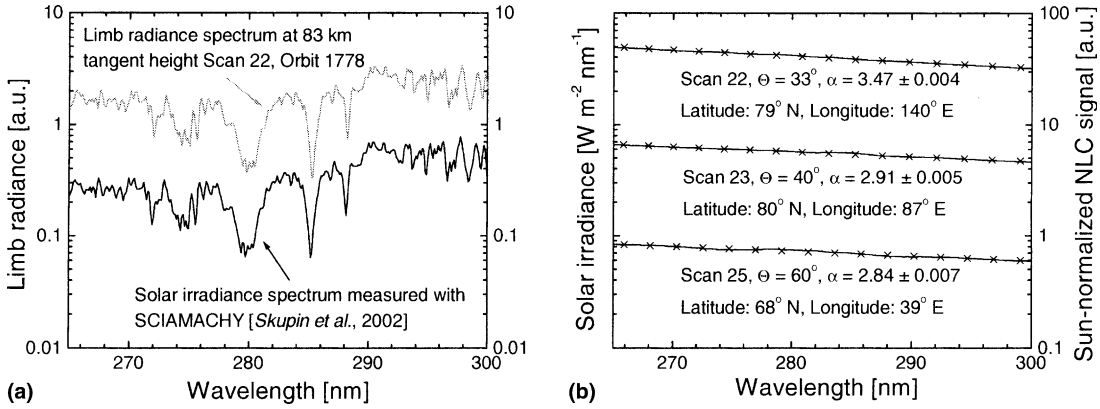

Fig. 3. Limb radiance spectrum for an NLC observation and solar irradiance spectrum (panel a) used to determine the spectral dependence of the sun-normalized NLC spectrum $i(\lambda, \Theta)$ (panel b). Panel (b) also shows power law functions (crosses) fitted to the measured sun-normalized NLC spectrum (solid lines).

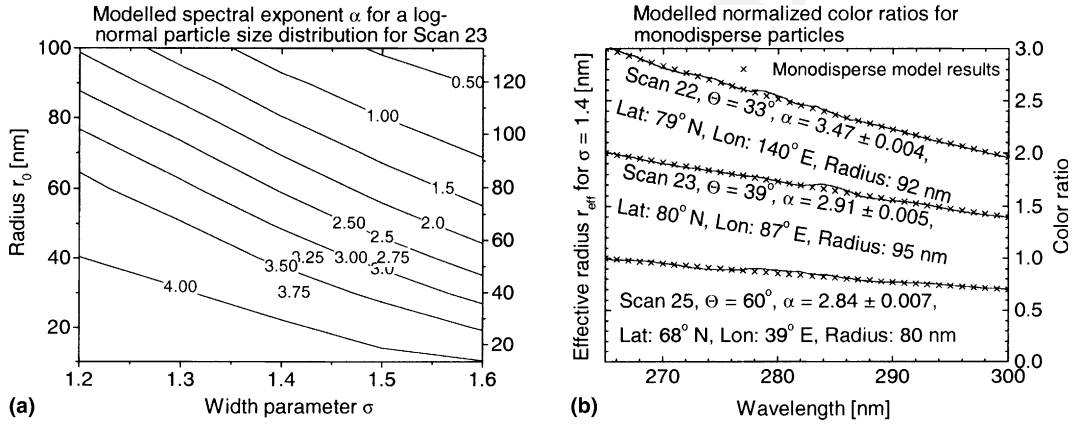

Fig. 4. Panel (a): theoretical dependence of the spectral exponent α on the log-normal PSD parameters r_0 and σ within the 265–300 nm spectral window for scattering angle of State 23. Panel (b): color ratios $c(\lambda)$ obtained from measurements (solid lines) and Mie calculations (crosses) for monodisperse NLCs (scaled by a factor of 2 for scan 23 and 3 for scan 22) to allow a better discrimination of the different spectra).

Skupin et al. (2003) solar irradiance spectrum (see Fig. 3(a)) as measured by SCIAMACHY was used as $S(\lambda)$. We found that the NLC differential scattering coefficient can be approximated by a power law $q(\lambda, \Theta) \propto \lambda^{-\alpha}$ with the spectral exponent α.

Fig. 3(b) shows a log–log plot of the sun-normalized NLC spectrum as a function of wavelength. The absolute of the slope corresponds to the spectral exponent α. The spectral points nicely follow a power law. Due to SCIAMACHY's hyperspectral capability the spectral exponents α can be determined with high fidelity. Note that the sun-normalized spectra $i(\lambda, \Theta)$ were smoothed with a 2 nm boxcar to remove the high frequency structures that arise mainly due to small wavelength misalignments. This high frequency component is not relevant for the determination of the spectral exponents. To infer information on the NLC particle sizes, the spectral exponents α obtained from SCIAMACHY observations are related to particle sizes by model calculations. For this we used the same assumptions as von Cossart et al. (1999) (see Section 1) and assumed that Eq. (1) is valid. The refractive index for ice was taken from Warren (1984). Fig. 4 shows model results of the spectral dependence of the differential scattering cross section for polydisperse NLCs (panel a) and monodisperse NLCs (panel b). Fig. 4a is a contour plot of the NLC spectral exponent for the 265–300 nm wavelength range as a function of r_0 and σ for the viewing geometry of limb scan 23 of orbit 1778. Fig. 4b gives the color ratios $c(\lambda) = \frac{i(\lambda)}{i(265nm)}$ for scans 22, 23, and 25 obtained from SCIAMACHY measurements. Also shown are Mie calculations for monodisperse spheres (i.e., $\sigma \to 0$ in Eq. (1)).

4. Discussion

The spectral exponent in Fig. 4(a) apparently depends on both r_0 and σ of the assumed log-normal distribution. A unique determination of both size distribution parameters requires at least three significantly different wavelengths (e.g., von Cossart et al., 1999). Due to

SCIAMACHY's wide spectral coverage, the determination of both r_0 and σ is in principle possible. Yet, this is difficult in practice since limb radiance profiles at visible wavelengths have to be employed. Generally, the unknown multiple scattering source function will make the accurate extraction of the NLC spectral signature difficult. Therefore, we limit ourselves to UV wavelengths here. The determination of both size parameters is presently under investigation. If we assume $\sigma = 1.4$ (von Cossart et al., 1999) (see Section 1), then the estimated value of r_0 of the NLC signature observed by SCIAMACHY is about $r_0 = 45$ nm for scan 22, i.e., within the typical range of NLC particle sizes. For scans 23 and 25 we obtain $r_0 = 50$ nm and $r_0 = 40$ nm, respectively. If we allow the width parameter σ to fall within the range 1.2–1.6. then the inferred radii are 25–65 nm for scan 22, 35–75 nm for scan 23, and 25–55 nm for scan 25.

If a monodisperse NLC model is used (Fig. 4(b)) then the radii that fit the observed normalized backscatter spectra best are 92 nm for scan 22, 95 nm for scan 23 and 80 nm for scan 25. Interestingly, the radii obtained from the monodisperse model are approximately twice as large as the radii from the polydisperse model assuming a log-normal distribution and $\sigma = 1.4$. The fact that the monodisperse radii are greater than the polydisperse ones is not surprising, since the scattering cross section scales as the squared volume of the particle in the Rayleigh limit, i.e., larger particles scatter more efficiently, and therefore they dominate the total scattering cross section. We found that the observed NLC backscatter spectra can be modeled very accurately with both a monodisperse and a polydisperse model. A similar result was recently obtained by Gumbel and Witt (2001) who showed that the observed NLC phase functions can be explained using both monodisperse and polydisperse models. This amounts to an ambiguity of the method to determine NLC particle sizes and the question arises what model is to be used. Both models do not exactly represent the actual PSD. The log-normal PSD – which is the most common PSD used to infer NLC particle sizes from optical measurements – most likely overestimates the number of larger particles, since large particles actually fall out faster than smaller ones (e.g., Gumbel and Witt, 2001), although it nicely fits the multi-color LIDAR measurements by von Cossart et al. (1999). The monodisperse model is obviously inadequate. Yet, one could argue, – particularly since the actual PSD is unknown that one should employ the simplest model -that accurately describes the observations. Once a more realistic NLC PSD is found, the particle radii based on the monodisperse assumption can numerically and perhaps analytically be transformed to the more appropriate size parameter.

5. Conclusion

First results of SCIAMACHY observations of NLCs in the northern hemisphere during summer 2002 and estimations of the radii of the NLC particles are presented. The NLC backscatter spectrum $i(\lambda, \Theta)$ and its spectral exponent α between 265 and 300 nm were determined for several cases. NLC particle radii were estimated assuming both monodisperse and polydisperse ice spheres, and the observations are reproduced very accurately with both models. The deduced NLC particle radii fall within the range 40–50 nm assuming a log-normal particle size distribution with $\sigma = 1.4$ and between 80 and 95 nm based on the monodisperse model. SCIAMACHY continues the long-term observations of global NLC coverage started by SME and complemented by WINDII, and it has the unique potential of providing a long term archive of NLC occurrence, particle sizes and the variations thereof.

Acknowledgements

We are indebted to the entire SCIAMACHY team, whose efforts make all scientific analysis possible. We also thank ESA for providing the SCIAMACHY level 0 data used in this study. Parts of this work have been funded by the German Ministry of Education and Research BMBF (Grant 07UFE12/8) and the German Aerospace Centre DLR (Grant 50EE0027).

References

Alpers, M., Gerding, M., Höffner, J., et al. NLC particle properties from a five-color lidar observation at 54°N. J. Geophys. Res. 105, 12235–12240, 2000.

Baumgarten, G., Fricke, K.H., von Cossart, G. Investigation of the shape of noctilucent cloud particles by polarization lidar technique. Geophys. Res. Lett. 29, 13, 2002.

Bovensmann, H., Burrows, J.P., Buchwitz, M., et al. SCIAMACHY: mission objectives and measurement modes. J. Atmos. Sci. 56 (2), 127–150, 1999.

Debrestian, D.J., Lumpe, J.D., Shettle, E.P., et al. An analysis of POAM II solar occultation observations of polar mesospheric clouds in the southern hemisphere. J. Geophys. Res. 102 (D2), 1971–1981, 1997.

Donahue, T.M., Guenther, B., Blamont, J.E. Noctilucent clouds in daytime: circumpolar particulate layers near the summer mesopause. J. Atmos. Sci. 36, 515–517, 1972.

Evans, W.F.J., Laframboise, L.R., Sine, K.R., et al. Observations of polar mesospheric clouds in summer 1993 by the WINDII instrument on UARS. Geophys. Res. Lett. 22, 2793–2796, 1995.

Gumbel, J., Witt, G. Rocket-borne photometry of NLC particle populations. Adv. Space Res. 28 (7), 1053–1058, 2001.

Gumbel, J., Stegman, J., Murtagh, D.P., et al. Scattering phase functions and particle sizes in noctilucent clouds. Geophys. Res. Lett. 28, 1415–1418, 2001.

Hervig, M., Thompson, R.E., McHugh, M., et al. First confirmation that water ice is the primary component of polar mesospheric clouds. Geophys. Res. Lett. 28, 971–974, 2001.

Kaiser, J.W. Retrieval from limb measurements, Ph.D. Thesis, University of Bremen, 2001.

Kaiser, J.W., Burrows, J.P. Fast weighting functions for retrievals from limb scattering measurements, JQRST, paper, 2002 (in press).

Kokhanovsky, A. Optics of Light Scattering Media. Springer Verlag, Berlin, Heidelberg, New York, 2001.

McLinden, C.A., McConnell, J.C., Griffioen, E., et al. A vector radiative transfer model for the ODIN/OSIRIS project. Can. J. Phys. 80 (S1), 2002.

Petelina, S.V., Llewellyn, E.J., Lloyd, N.D., et al. Polar mesospheric clouds observed with the optical spectrograph on Odin in June–August, 2001 (Abstract), Eos. Trans. AGU, 82 (47), Fall Meet. Suppl., Abstract SA41B-0744, 2001.

'Rusch, D.W., Thomas, G.E., Jensen, E.J. Particle size distributions in polar mesospheric clouds derived from solar mesosphere explorer measurements. J. Geophys. Res. 96, 12933–12939, 1991.

Sioris, C., von Savigny, C., Gattinger, R.L., et al. Attitude determination for limb-scanning satellites: the ''knee at 305 nm (Abstract), Eos. Trans. AGU, 82(47), Fall Meet. Suppl., Abstract A32B-0056, 2001.

Skupin, J., Noël, S., Wuttke, M.W., et al. In-flight calibration of the SCIAMACHY solar irradiance spectrum. Adv. Space Res., 32, 2002 (submitted).

Thomas, G.E., Oliviero, J.J. Climatology of polar mesospheric clouds, 2. further analysis of solar mesosphere explorer data. J. Geophys. Res. 94 (D12), 14,673–14,681, 1989.

Thomas, G.E. Mesospheric clouds and the physics of the mesopause region. Rev. Geophys. 29, 553–575, 1991.

von Cossart, G., Fiedler, J., von Zahn, U. Size distributions of NLC particles as determined from 3-colour observations of NLC by ground-based lidar. Geophys. Res. Lett. 26, 1513–1516, 1999.

Warren, S.G. Optical constants of ice from the ultraviolet to the microwave. Appl. Opt. 23, 1206–1225, 1984.

Witt, G., Dye, J.E., Wilhelm, N. Rocket-borne measurements of scattered sunlight in the mesopause. J. Atmos. Terr. Phys. 38, 223–238, 1976.